Progress In Electromagnetics Research, Vol. 126, 333–353, 2012

FAST 3-D MICROWAVE IMAGING METHOD BASED ON SUBAPERTURE APPROXIMATION

K.-F. Liao*, X.-L. Zhang, and J. Shi

School of Electronic Engineering, University of Electronic Science and Technology of China, Chengdu 611731, China

Abstract—In this paper, the subaperture approximation (SA) method for 3-D microwave imaging is presented based on the sparsity of 3-D image. The idea is that the sparsity information can be extracted from the lower resolution image obtained using the subaperture of the (virtual) array and be used for high-resolution imaging to reduce the imaging region. Thus, a recursion procedure that can significantly reduce the computational cost is established. Compared with the surface-tracing-based method, the SA method can avoid the loss of isolated scatterers. The feasibility is verified by using experimental data. After analysis, the SA method can reduce the computational cost from two aspects: reducing the array element number needed to be processed and the pixels needed to be processed. The computational cost is mainly related to the target characteristics (the sparsity ratio and the topological structure), and decreases with the increase of the sparsity ratio. When the sparsity ratio is larger than 97.6%, the computational cost can be lower than 10% of the 3-D back-projection (BP) method.

1. INTRODUCTION

Because of its potential applications in remote sensing, radar cross section (RCS) measurement, concealed weapon detection and through-barrier imaging, 3-D microwave imaging is becoming an increasing interest in the field of radar in recent years [1–7]. The basic idea of 3-D microwave imaging is using a 2-D array to cause 2-D resolution in 2-D array plane, together with the pulse compression technique to obtain 3-D resolution. To reduce the system cost, the 2-D array is implemented by using synthetic aperture technique, such as circle synthetic aperture

Received 11 January 2012, Accepted 7 March 2012, Scheduled 21 March 2012

* Corresponding author: Ke-Fei Liao (liaokf@yahoo.cn).

radar (SAR) [8, 9], elevation circular SAR [10], curve SAR [11], and linear array SAR [12].

Many imaging methods have been developed for 3-D microwave imaging, such as 3-D back-projection (BP) method [13], 3-D range migration algorithm [14, 27] and chirp scaling algorithm [15]. However, one of the main disadvantages of 3-D microwave imaging methods is their high computational cost. In practice, many 3-D imaging regions contain no scatterer or are shadowed by other scatterers, with typical sparsity. Thus, the surface-tracing-based (STB) 3-D imaging method had been proposed [16], which models the 3-D image as a continuous surface and traces the surface by using multiresolution approximation (MA) technique, which can reduce the computational cost significantly.

But in some cases, especially in the RCS measurement and concealed weapon detection application, the 3-D image is a collection of isolated scatterers rather than a continuous surface [17, 18]. Thus, the surface tracing technique might lose some isolated scatterers and becomes invalid.

A fast 3-D microwave imaging method based on subaperture approximation (SA) is presented in this paper, whose basic idea is to obtain a low-resolution image by using a subaperture firstly (according to the antenna theory [19], the image resolution is inverse ratio to the aperture size), to use the low-resolution image as the prior information [28] to reduce the imaging region, to obtain a higher-resolution image by expanding subapertures, and to obtain a fine-resolution image iteratively. Compared with the STB method, there is no scatterer lost during processing, which is more feasible for the RCS measurement and concealed weapon detection application.

This paper is organized into 5 sections. In Section 2, the principle of typical 3-D microwave imaging (SAR) is introduced. In Section 3, the principle and fundamental stages of SA 3-D imaging method are discussed, and the experimental results are obtained. The computational cost is analyzed in Section 4. Finally, a summary is given in Section 5.

2. PROBLEM FORMULATION

To achieve high-resolution, the size of 2-D array of 3-D microwave imaging system is large, whose cost is huge. To reduce the system cost, the synthetic aperture technique (such as circle SAR, elevation circular SAR, curve SAR, and linear array SAR) and sparse array technique are applied. In essence, both of them can be explained using the array theory. The signal model, imaging method and sparsity of typical 3-D microwave imaging (SAR) will be introduced in this section.

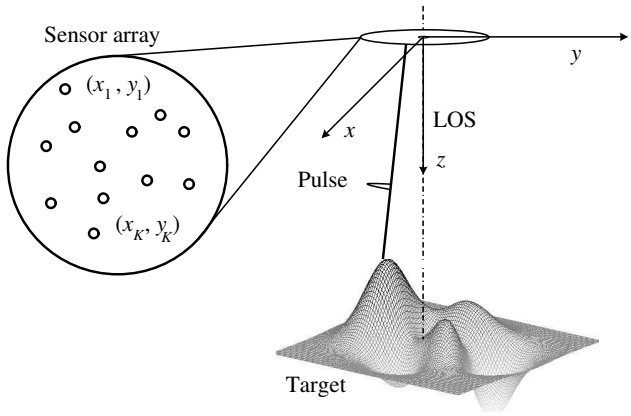

Figure 1. Geometry of 3-D microwave array imaging.

2.1. Signal Model

The geometry of 3-D microwave array imaging is shown in Figure 1. An array transmits a series of electromagnetic (EM) waves to the observed target and receives the echoes. The positions of the array elements can be described as element position set (EP set, denoted as $\mathbf{P}_e$):

$$\mathbf{P}_e = \left\{ \mathbf{p}_e^k \middle| \mathbf{p}_e^k = \langle x_k, y_k, z_0 \rangle; \quad k \in \Pi \right\} \tag{1}$$

where $\langle x_k, y_k, z_0 \rangle$ denotes the kth element's position, Π the index set, $\Pi = \{1, 2, \ldots, K\}$, and K the total number of the array elements.

The slant range from the nth single scatterer with position $\mathbf{p}_n$ to the array element with position $\mathbf{p}_e^k$ is:

$$R\left(\mathbf{p}_n, \mathbf{p}_e^k\right) \triangleq 2 \left\| \mathbf{p}_e^k - \mathbf{p}_n \right\|_2 \tag{2}$$

where $\|\cdot\|_2$ denotes the 2-norm of vector.

The single scatterer's echo $\mathbf{d}(t, k; n)$ can be written as:

$$\mathbf{d}(t, k; n) = e^{j\kappa_0 R(\mathbf{p}_n, \mathbf{p}_e^k)} \chi^R \left(t - R\left(\mathbf{p}_n, \mathbf{p}_e^k\right) \right) \tag{3}$$

where κ_0 denotes the wave number, $\kappa_0 = 2\pi/\lambda$, λ the wave length of the carrier, t the range domain, and $\chi^R(t)$ the ambiguity function after range compression in the range direction.

The first term in Equation (3) causes the resolving in the x and y directions, whose angular resolutions ρ_x and ρ_y can be calculated as [6, 13]:

$$\rho_x = \lambda / 2L_x \tag{4a}$$

$$\rho_y = \lambda / 2L_y \tag{4b}$$

where L_x and L_y denote the effective aperture lengths in the x and y directions, respectively.

The second term in Equation (3) causes the resolving in the range direction. The ambiguity function $\chi^R(t)$ could be regarded as sinc function for pulse-compression radar, whose resolution ρ_r can be calculated respectively as:

$$\rho_r = c/2B \tag{5}$$

where c denotes the speed of light and B the bandwidth of pulse-compression radar.

For a multiple-scattering target, denoted as Ξ, its echo is the sum of all scatterers, i.e.,

$$\mathbf{D}(t,k) = \sum_{\mathbf{p}_n \in \Xi} \sigma_n \mathbf{d}(t,k;n) \tag{6}$$

where σ_n denotes the scattering coefficient of the nth scatterer.

2.2. Imaging Method and Analysis

Because of its generality, the back-projection (BP) method [13] has become a popular and effective technique for 3-D microwave imaging.

The BP method chooses one pixel, calculates its ranges to the transmitters and receivers, selects the range-compressed echoes correspond to the pixel, compensates its phases, and accumulates the echoes.

Given a pixel $\mathbf{p}_n$, its output $\mathbf{I}[\mathbf{p}_n]$ of BP operator is presented in Equation (7):

$$\mathbf{I}[\mathbf{p}_n] \triangleq \sum_{k=1}^{K} \mathbf{D}(t,k) e^{-2j\kappa_0 R(\mathbf{p}_n, \mathbf{p}_e^k)} \tag{7}$$

According to Equation (7), the 3-D BP method can be divided roughly into four steps: range-compression, interpolation, resampling, and coherent summation. For the whole imaging regions Ω, the BP method traverses the whole region pixel by pixel (see more details in [13]).

According to Equation (7), ignoring the computational cost of the range-compression operation, for a 3-D imaging region with size $X \times Y \times Z$ (pixel^3), the computational cost of 3-D BP method is:

$$\Psi_{\mathrm{BP}} = XYZ\Psi_b \tag{8}$$

where Ψ_b denotes the computational cost of the single-scatterer BP operator defined in Equation (7), which can be calculated as:

$$\Psi_b = K\left(\Psi_{int} + \Psi_{coh}\right) \tag{9}$$

where Ψ_{int} and Ψ_{coh} denote the computational costs of the interpolation and coherent summation operations respectively, which can be considered as constants during the analysis of computational cost.

From Equations (8), (9), we can find that there are two reasons that the computational cost of the 3-D BP method is far greater than that of 2-D BP method in the same resolution and image scene.

2.2.1. Increase of Acquired Data

The 2-D microwave imaging system, typically SAR [21, 22], uses a linear array (typically thousands to tens of thousands virtual elements for one pixel) to cause azimuth resolution. The 3-D imaging system [8–12] has to use a 2-D sensor array (typically hundreds of thousands to millions (virtual) elements for one pixel) to cause 2-D resolution, i.e., we need more cost to process a pixel for 3-D imaging system.

2.2.2. Expansion of Imaging Space

Compared with 2-D imaging system, the imaging space of 3-D imaging system expands to three dimensions, which means that more pixels are needed to be processed during imaging, increasing the computational cost correspondingly.

To reduce the computational cost, the subaperture approximation method is presented in this paper.

3. SA 3-D IMAGING METHOD

Unlike the 2-D imaging problem, 3-D imaging problem behaves sparsely [17, 18, 24–26]. Thus, the STB 3-D imaging method was proposed [16]. However, when the sparse images are collections of isolated scatterers rather than a continuous surface, the STB method becomes invalid. To solve this problem, the subaperture approximation (SA) 3-D imaging method is discussed in this section, which is available for reducing the computational cost and imaging non-continuous - surface target.

3.1. Principle of SA 3-D Imaging Method

As discussed in last section, the BP method processes the imaging space pixel by pixel. Because of the sparsity of 3-D image, there is no scatterer in the vast region of the imaging space. Consequently, a large proportion of BP operation is useless provided that the positions of scatterers are known.

The prior information of scatterers' positions can be extracted by using the MA technique [20].

The foundation of SA method is the relationship between the aperture size and image resolution, i.e., the resolution is inverse ratio to the aperture size. Thus, the prior information needed for the higher resolution imaging can be extracted from the lower resolution image obtained using the subaperture of the array, as shown in Figure 2.

Firstly, the SA method selects a subaperture (left in Figure 2), obtains a low-resolution image of the entire imaging region, and picks out region of interest (ROI) that contains the possible scatterers. Then, it focuses on ROI with a larger subaperture (middle in Figure 2) and obtains a higher resolution image. Thirdly, it expands subapertures iteratively until full aperture (right in Figure 2) and obtains a fine-resolution image finally.

Note that, because the resolution in the line-of-sight direction (LOS) is related to the signal bandwidth, the SA technique can only be used in the array direction but not in the LOS direction.

Like the STB method, the SA method uses the idea of MA. The difference between them is the way to obtain low-resolution image.

The STB method images using the full aperture and samples the high-resolution image with different intervals to obtain low-resolution image. When the scatterers are in continuous surface, shown as area A in Figure 3(a), it works well. But when there are some isolated scatterers, the STB method might lose some of them during the

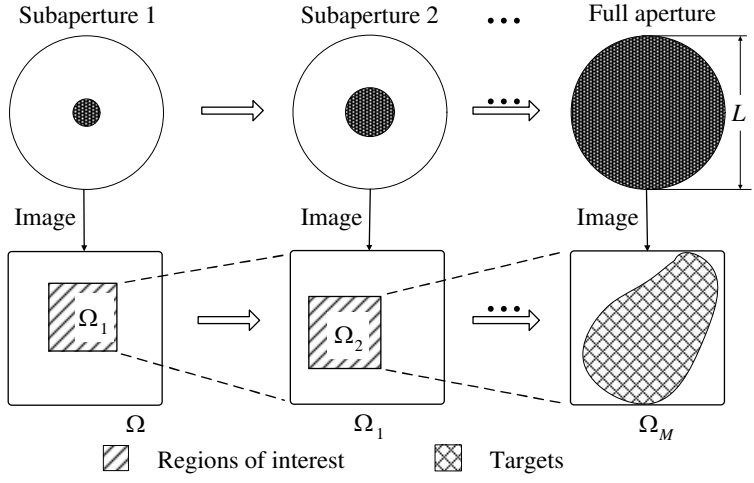

Figure 2. Schematic diagram of SA 3-D imaging method.

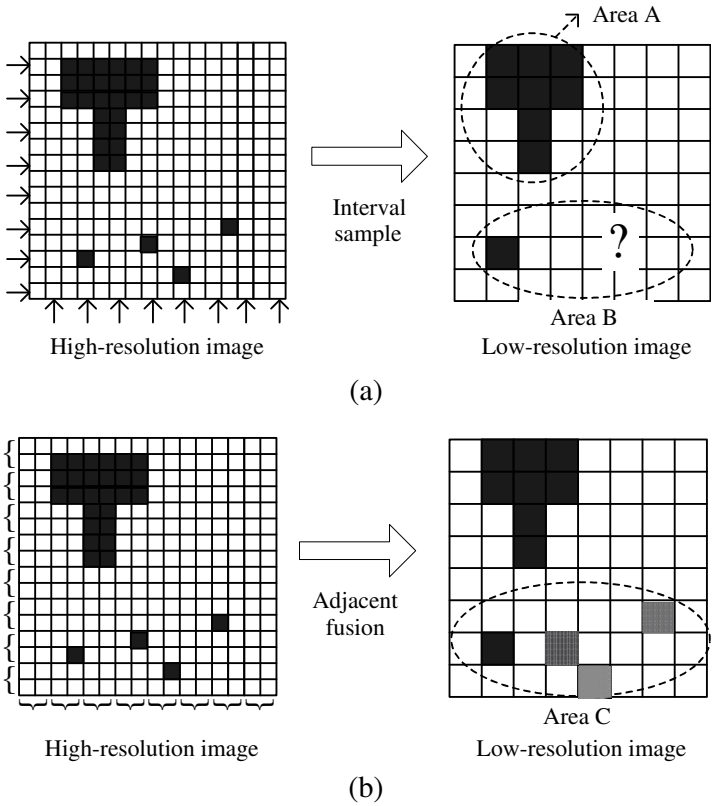

Figure 3. Comparison between the MA of STB and SA methods. (a) STB method. (b) SA method.

sampling, shown as area B in Figure 3(a).

To overcome this problem, the subaperture imaging is used in SA method. Choosing the resolution corresponding to the subaperture as the pixel interval, according to the antenna theory [19], the scattering coefficient of one pixel is the integral of the scattering coefficients over the corresponding resolution cell. As a result, the SA method can avoid the loss of scatterers during course of MA, shown as area C in Figure 3(b).

Moreover, by using the idea of MA, the SA method can use different resolutions for different parts of the scene to obtain a better effect by avoiding the loss of scatterers, which will be researched in further articles.

3.2. Steps of SA Method

Denoting the 3-D imaging region as Ω, the size of full aperture as L, and the resolution of full aperture imaging as ρ_L, the main steps of SA method are presented as follows:

Step 1 Initiation imaging

Select a subaperture whose size is l_1 ($l_1 < L$), and the resolution ρ_1 of subaperture l_1 is:

$$\rho_1 = \rho_L L / l_1 \tag{10}$$

Partition the imaging space using ρ_1 and obtain the initial-resolution image by BP method.

Step 2 ROI selection

Find the maximum pixels' scattering coefficient $\sigma_{\max}^{[1]}$ in the initial image, select a threshold Θ, and pick out the ROI Ω_1, whose pixels' scattering coefficients (absolute values) are larger than $\Theta|\sigma|_{\max}^{[1]}$, i.e.,

$$\Omega_1 = \left\{ \mathbf{p} \,||\mathbf{I}(\mathbf{p})| > \Theta \,|\sigma|_{\max}^{[1]}, \quad \mathbf{p} \in \Omega \right\} \tag{11}$$

Step 3 Higher-resolution imaging

Expand the size of subaperture l_1 to l_2 ($l_1 < l_2 \leq L$), and the resolution ρ_2 of subaperture l_2 is:

$$\rho_2 = \rho_L L / l_2 \tag{12}$$

Partition the ROI Ω_1 using ρ_2 and obtain the higher-resolution image of Ω_1 using Equation (7) pixel by pixel.

Step 4 Recursion

Replace $\sigma_{\max}^{[1]}$, l_2 and Ω_1 in steps 2–3 by $\sigma_{\max}^{[j]}$, l_{j+1} and Ω_j, where j denotes the recursion index, $j = 2, \ldots$, and repeat the steps 2–3 until obtaining the fine-resolution image finally.

Note that the BP method is used to help imaging and can be replaced by other suitable imaging methods, such as 3-D range migration algorithm [14] and compressed sensing imaging method [23].

In step 2, the threshold Θ is a key parameter to balance the computational cost and image details loss. From Equation (11), we see that the smaller Θ is, the more scatterers are picked into ROIs, the less image details lose, and the higher the computational cost is. Contrariwise, the larger Θ is, the lower the computational cost is.

In practice, Θ can be selected based on the peak side-lobe ratio (PSLR). For an imaging system whose PSLR is given, the threshold should be slightly lower than the designed PSLR, because if Θ is far smaller than the PSLR, many side-lobes are selected into the ROIs and the ROIs unnecessarily widened; if Θ is higher than the PSLR, some image details might be lost during the course of ROI selection.

3.3. Experimental Results

The feasibility of the SA method is verified using the experimental data (the source comes from literature [17], and the size of virtual array is

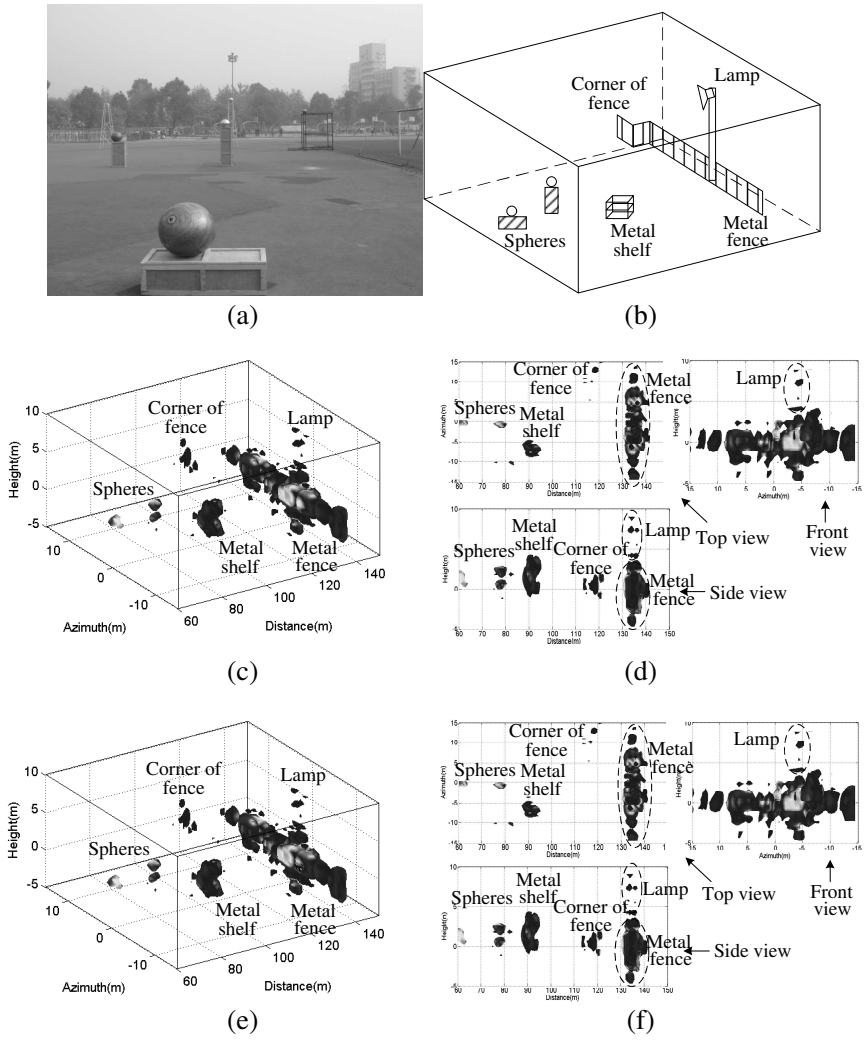

Figure 4. (a) Photograph of image scene. (b) Diagrammatic map of image scene. (c) Imaging result of 3-D BP method. (d) Side-view, top-view and front-view images of 3-D BP method respectively. (e) Imaging result of SA method. (f) Side-view, top-view and front-view images of SA method respectively.

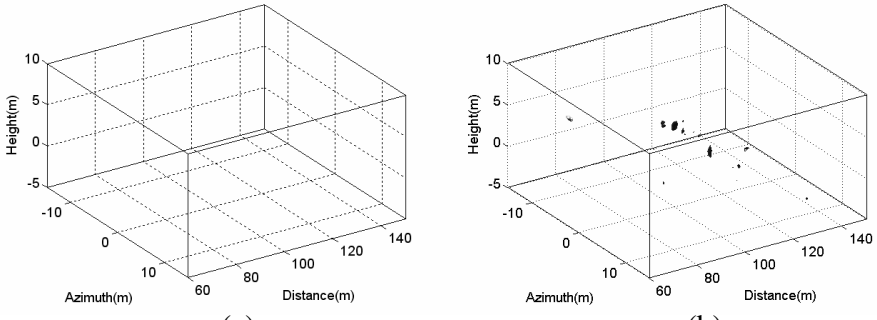

Figure 5. The images by subtracting the SA image from the 3-D BP image when showed the scatterers whose (absolute) value are (a) above −13 dB; (b) above −30 dB.

2 m × 2 m).

Figure 5(a) is the photograph of image scene, and main targets are illustrated in Figure 4(b). Figures 4(c), (d) are the imaging results using the 3-D BP method in 3-D view, side-view, top-view and front-view, respectively. From Figures 4(c), (d), we find that the targets only occupy a small part of 3-D image region, which shows the typical sparsity (99.03% of imaging regions has no scatterer).

Figures 4(e), (f) are the imaging results using the SA method in 3-D view, side-view, top-view and front-view, respectively.

The difference between the imaging results of 3-D BP method and SA method is shown in Figures 5(a), (b) by subtracting the SA image (Figure 4(e)) from the 3-D BP image (Figure 4(c)). No scatterer's (absolute) value is above −13 dB of maximum image (absolute) value (the same as the system designed PSLR) as shown in Figure 5(a), but a few scatterers' (absolute) values are above −30 dB as shown in Figure 5(b). In fact, the maximum (absolute) value in Figure 5(b) is −23.24 dB of that in Figure 4(c), far below the PSLR, which means no scatterers lost in process of SA method.

As results, we can conclude that:

- The SA method can reconstruct the scene correctly.
- By selecting proper threshold, the imaging quality of SA method is the same as 3-D BP method.
- The system designed PSLR is a proper threshold, which can avoid scatterers lost and keep ROIs exact.

4. COMPUTATIONAL COST AND DISCUSSION

During the research, we find that the selection of subaperture, topological structure and sparsity ratio of the target affect the computational cost of SA method significantly. In this section, its computational cost is discussed in detail.

4.1. Effect of Subaperture Selection

Two typical subaperture selection strategies, linear expansion and 2-base expansion, are deduced in this subsection.

4.1.1. Linear Expansion

Assuming that the size of full aperture is L, we linearly expand the sizes of subapertures $l_m = mL/M$ in recursion, where m denotes the mth recursion, $m = 1, 2, \ldots, M$, and M denotes the recursion number, $l_M = L$.

For a 3-D imaging region with final size $X \times Y \times Z$ (pixel^3), the number of scatterers is:

$$\Phi = (1 - G)XYZ \tag{13}$$

where G denotes the sparsity ratio, which means the ratio of the number of pixels of the region without scatterers to that of the entire image region.

Because of the reducing of the resolution corresponding to the mth recursion's subaperture, the number of pixels of the ROI in the mth recursion is:

$$\Phi^{[m]} = (\rho_m/\rho_L)^2(1 - G_m)XYZ = (m/M)^2(1 - G_m)XYZ \tag{14}$$

Note that, in fact, the topological structure of the target will affect the number of pixels of the ROI, which will be discussed in the next subsection. Herein we assume that the target has isolated structure, thus the ROI varies linearly with the number of scatterers and the square of system resolution.

On the other hand, assume that the array elements distribute uniformly in the (virtual) array. Because of the adoption of subapertures, the computational cost $\Psi_{\mathrm{SA}}^{[m]}$ of the single-scatterer SA method in the mth recursion is:

$$\Psi_{\mathrm{SA}}^{[m]} = (m/M)^2\Psi_b \tag{15}$$

As a result, its computational cost in the mth recursion is:

$$\Psi_{\mathrm{SA}}^{[m]} = (m/M)^2(1 - G_m)XYZ\Psi_s^{[m]} = (m/M)^4(1 - G_m)XYZ\Psi_b \tag{16}$$

Consequently, the total computational cost of SA method is:

$$\Psi_{\mathrm{SA}} = \sum_{m=1}^{M} \Psi_{\mathrm{SA}}^{[m]} \tag{17}$$

Since the size $X \times Y \times Z$ (pixel^3) and Ψ_b keep constant during one imaging task, the sparsity ratio G and recursion number M mainly determine the computational cost.

According to the discussion above, the SA method can reduce the computational cost than 3-D BP method by two ways:

◊ From Equation (14), we find that it reduces the pixels of 3-D imaging region needed to be processed.

◊ From Equation (15), we find that it reduces the element number of sensor array needed to be processed.

- 2-base expansion

Expand the sizes of subapertures by power of 2, i.e., $l_m = L/2^{M-m}$ during recursion.

By a similar derivation, we have the total computational cost of SA method:

$$\Psi_{\mathrm{SA}} = \sum_{m=1}^{M} 2^{-4(M-m)}(1-G)XYZ\Psi_b \tag{18}$$

The difference between linear expansion and 2-base expansion will be discussed in Section 4.3 by numerical experiments.

4.2. Effect of Topological Structures

Generally speaking, according to the principle of SA method, the sparser the image scene is, the smaller the ROI is, and the lower the computational cost is. In practice, however, the topological structure of target also affects the computational cost. For any targets, it could be considered as one of three kinds of topological structures, or their combination.

4.2.1. Zero-dimensional Structure

The 0-D structure means a collection of isolated scatterers (whose sizes are smaller than the system resolution, such as metal spheres in Figure 4(c)). For every scatterer of this structure, there exists a zero-scattering-coefficient neighborhood as shown in Figure 6(a).

To describe how much the topological structure affects the computational cost, we denote Ξ as the ROI search efficiency, which

means the ratio of the number of pixels of the target area to that of the ROI area when the resolution is doubled in recursion. The higher Ξ is, the lower the computational cost is.

Assume that the number of pixels of target is n in scene. Thus, every pixel produces an independent ROI during the recursion as shown in Figures 6(b), (c), and the ROI area is $4n$ when resolution is doubled. In doubled-resolution image, the target area is n. As a result, the ROI search efficiency is 25% (see Figures 6(c), (d)).

4.2.2. One-dimensional Structure

The 1-D structure means a continuous line (whose length of a side is smaller than the system resolution, and length of another side is far larger than the system resolution, such as the lamp in Figure 4(c)). The scatterers of this structure combine a continuous line as shown in Figure 7(a).

During the recursion, the ROIs of scatterers overlap to each other along the line as shown in Figures 7(b), (c). Assume that the number of pixels of target is n in scene and target's edge effect ignored. Thus, the ROI area is n, and the target area is $n/2$. Thus, the ROI search efficiency is 50% (see Figures 7(c), (d)).

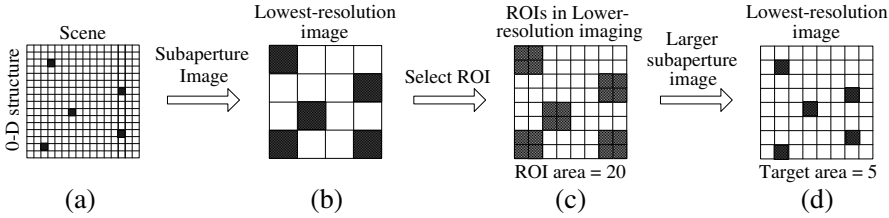

Figure 6. Zero-dimensional topological structure produces independent ROIs, whose search efficiency is 25%.

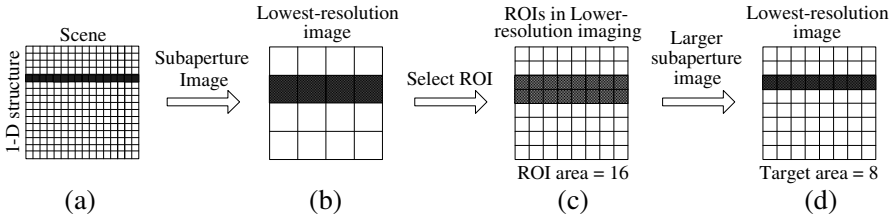

Figure 7. One-dimensional topological structure, whose ROIs overlap to each other along the line and search efficiency is 50%.

4.2.3. Two-dimensional Structure

The 2-D structure, such as buildings, vehicles, etc. (whose sizes are far larger than the system resolution) means a continuous surface. The scatterers of this structure combine a continuous region, which is shown as Figure 8(a).

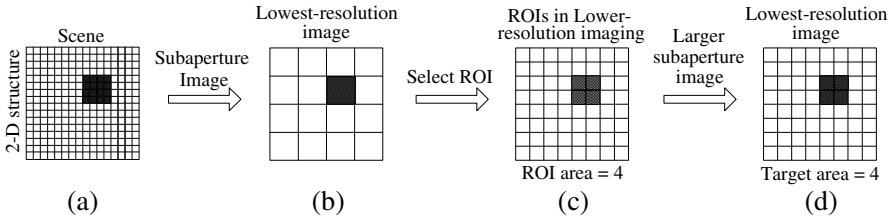

Figure 8. Two-dimensional topological structure, whose ROIs overlap to each other to combine a continuous surface and search efficiency is 100%.

During the recursion, the ROIs of scatterers overlap to each other and combine a continuous surface as shown in Figures 8(b), (c). Assume that the pixel (scatterer) number of target is n in scene and target's edge effect ignored. Thus, the ROI area is $n/4$, and the target area is $n/4$. Thus, the ROI search efficiency is 100% (see Figures 8(c), (d)).

As results, different structures produce different ROIs, which affect the ROI search efficiency. Furthermore, by comparing the ROIs' areas, we conclude that the 2-D structure has the highest search efficiency, 0-D structure the lowest search efficiencyand 1-D structure the search efficiency between the former two. Note that the topological structure of the same target may change under different resolution conditions. As a result, for any targets, the computational cost is within the 0-D structure's and 2-D structure's ranges.

In the next subsection, the computational cost of these three structures will be analyzed in detail by numerical experiments.

4.3. Numeral Simulation Analysis

In this section, the effect of the subaperture selection, topological structure and sparsity on the computational cost is analyzed in detail by using numerical simulation.

4.3.1. Subaperture Selection

According to the analysis in Section 4.1, different subaperture selections (typically linear expansion and 2-base expansion) cause different computational cost expressions, whose numerical simulation results are shown in Figures 9 and 10, respectively.

The sparsity ratio in recursion is related to the subaperture, as suggested in Figures 9(a) and 10(a), from which we can find that as the subapertures expand, the sparsity ratios of recursions approach to that of BP method ($G = 99\%$), i.e., the ROIs approach to the exact target. The difference among subaperture selections is that they have different rates of approaching ROIs, and the 2-base expansion approaches quickly than the linear expansion because of the longer steps of subapertures. However, the shorter steps of the linear

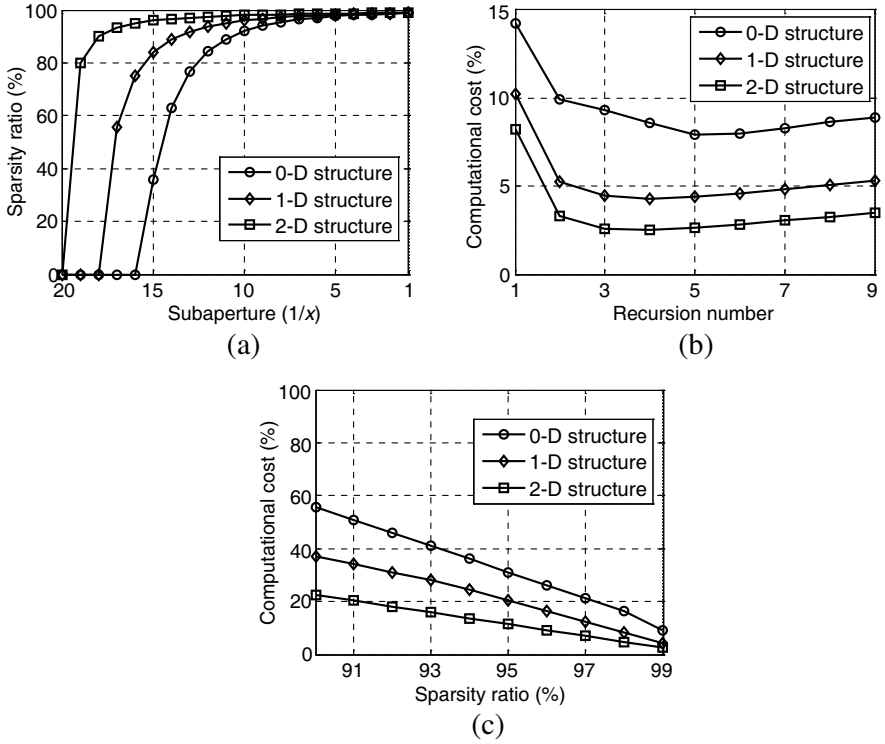

Figure 9. Computational cost analysis of linearly expansion of subapertures. (a) Relationship between subapertures and sparsity ratios. (b) Computational cost ratio with different recursion numbers. (c) Computational cost ratio with different sparsity ratios.

expansion mean more exact search of ROIs.

The ratios of the computational cost of the SA method to that of 3-D BP method with different recursion numbers M are plotted in Figures 9(b) and 10(b). The linearly expansion has lower computational cost than the 2-base expansion. Plus, having the shorter steps of subapertures which benefits exact search of ROIs, the linear expansion is used more often.

Moreover, in the linear expansion, the computational cost reaches the lowest points when $M = 5$ in the 2-D structure and $M = 3$ in the 0-D structure (see Figure 9(b)), which are the best choices of M. In the 2-base expansion, the computational cost decreases as M increases, and when $M > 2$, the decrease is insignificant (see Figure 10(b)), thus, $M = 2$ is an appropriate value. As a result, we can conclude that once

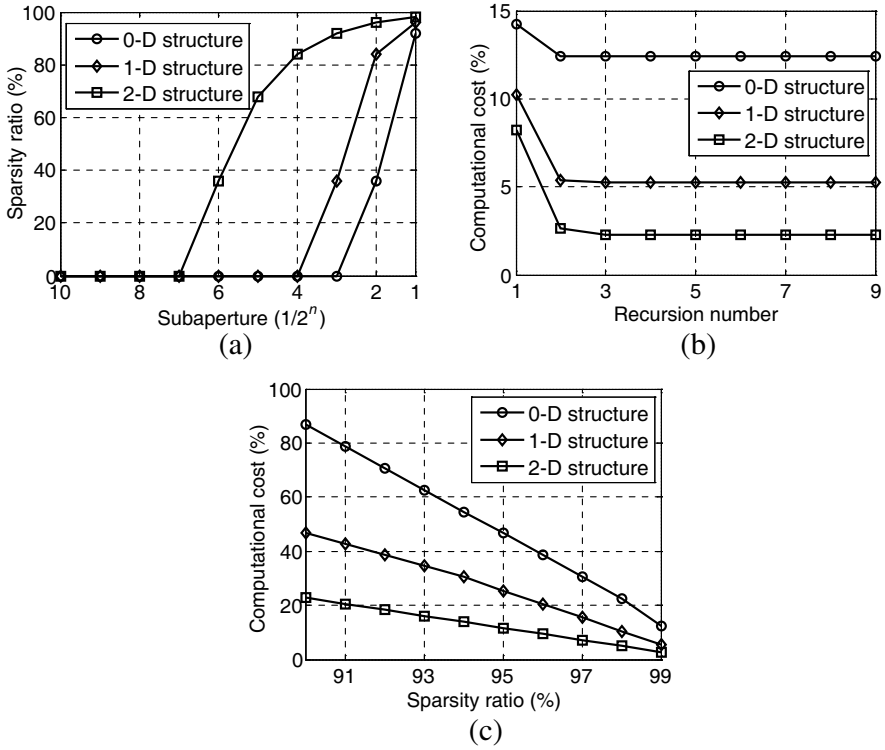

Figure 10. Computational cost analysis of 2 base expansion of subapertures. (a) Relationship between subapertures and sparsity ratios. (b) Computational cost ratio with different recursion numbers. (c) Computational cost ratio with different sparsity ratios.

we know how to select the subapertures, the best choice of M can be decided.

4.3.2. Topological Structure

As concluded in last subsection, the ROI search efficiency ratio of 0-D, 1-D and 2-D structures is $1:2:4$ (under the conditions that resolution is doubled). This result is supported by numerical simulation as shown in Figures 9 and 10, from which we can find that the 0-D structure has the highest computational cost, the 2-D structure the lowest computational cost, and the 1-D structure the computational cost between the former two. Note that because the computational cost shown here is the sum of all recursions and because targets have edge effects, the ratio is not exact $1:2:4$.

4.3.3. Sparsity Ratio

Once the subaperture selection and topological structure of target are known, the computational cost is only related to the sparsity ratio. By selecting the sub-scenes, we can correspondingly vary the sparsity ratio G, and the ratios of the computational cost of the SA method to that of 3-D BP method with different G are plotted in Figures 9(c) and 10(c).

From these figures we can find that the computational cost decreases linearly as the sparsity ratio increases. Take the linear expansion for example, the computational cost is lower than 55% of the 3-D BP method when $G_M > 90\%$ in the worst situation (0-D structure), and lower than 10% of the 3-D BP method when $G_M > 97.6\%$ in average situation (1-D structure).

In experimental data as we stated in Section 3.3 ($G \approx 99.03\%$), the computational cost of SA method is about 8.61% of 3-D BP method, within the ranges of 0-D and 1-D structures. This means that the practical target is a combination of two or three topological structures, which verifies the analysis of the three topological structures.

5. CONCLUSIONS

The concept of SA method for 3-D microwave imaging has been introduced in this paper, which can work well in 3-D topographic mapping, RCS measurement and concealed weapon detection application, etc. With the SA method, it is possible to reduce the computational cost of 3-D microwave imaging significantly. Basically, the SA method uses a subaperture to obtain a low-resolution image and

extract the sparsity information for high-resolution imaging to reduce the imaging region. The SA method can avoid the loss of scatterers during the course of multiresolution approximation compared with the STB method. The feasibility of SA method and avoiding the loss of scatterers have been verified by using experimental data.

Because of the adoption of subaperture, the SA method can reduce computational cost from two aspects: reducing the element number of sensor array needed to be processed and the pixels of 3-D imaging regions needed to be processed. According to the comparison of subapertures selection methods and three topological structures, we had found that once we know the subaperture selection, the computational cost is only related to the target characteristics (the topological structure and the sparsity ratio). When the sparsity ratio is larger than 97.6%, the computational cost of SA method is lower than 10% of the 3-D BP method in average situation.

ACKNOWLEDGMENT

This work was supported by the National Natural Science Foundation of China (Grant No. 61101170) and Ph.D. Programs Foundation of Ministry of Education of China (No. 2011018511001).

The authors are with Lab. B504, School of Electronic Engineering, University of Electronic Science and Technology of China, 610054, Chengdu, P. R. China.

REFERENCES

1. Li, F., X. Chen, and K.-M. Huang, "Microwave imaging a buried object by the GA and using the S_{11} parameter," *Progress In Electromagnetics Research*, Vol. 85, 289–302, 2008.
2. Zhou, H., T. Takenaka, J. Johnson, and T. Tanaka, "A breast imaging model using microwaves and a time domain three dimensional reconstruction method," *Progress In Electromagnetics Research*, Vol. 93, 57–70, 2009.
3. Ren, X.-Z., L. H. Qiao, and Y. Qin, "A three-dimensional imaging algorithm for tomography SAR based on improved interpolated array transform," *Progress In Electromagnetics Research*, Vol. 120, 181–193, 2011.
4. Li, N.-J., C.-F. Hu, Y.-X. Zhao, and J. J. Wei, "A new method of near-field three dimensional synthetic aperture radar imaging," *PIERS Proceedings*, 71–74, Cambridge, USA, Jul. 5–8, 2010.

5. Li, C. and D.-Y. Zhu, "A residue-pairing algorithm for InSAR phase unwrapping," *Progress In Electromagnetics Research*, Vol. 95, 341–354, 2009.
6. Klare, J., "Digital beamforming for a 3D MIMO SAR — Improvements through frequency and waveform diversity," *IGARSS 2008*, V17–V20, Boston, MA, United States, Jul. 2008.
7. Teng, H. T., H.-T. Ewe, and S. L. Tan, "Multifractal dimension and its geometrical terrain properties for classification of multi-band multi-polarized SAR image," *Progress In Electromagnetics Research*, Vol. 104, 221–237, 2010.
8. Yu, L. and Y. Zhang, "CSAR imaging with data extrapolation and approximate GLRT techniques," *Progress In Electromagnetics Research M*, Vol. 19, 209–220, 2011.
9. Chan, T.-K., Y. Kuga, and A. Ishimaru, "Experimental studies on circular SAR imaging in clutter using angular correlation function technique," *IEEE Trans. Geoscience and Remote Sensing*, Vol. 37, No. 5, 2192–2197, Part 1, Sep. 1999.
10. Bryant, M. L., L. L. Gostin, and M. Soumekh, "3-D E-CSAR imaging of a T-72 tank and synthesis of its SAR reconstructions," *IEEE Trans. Aerospace and Electronic Systems*, Vol. 39, No. 1, 211–227, Jan. 2003.
11. Axelsson, S. R. J., "Beam characteristics of the three-dimensional SAR in curved or random paths," *IEEE Trans. Geoscience and Remote Sensing*, Vol. 42, No. 10, 2324–2334, Oct. 2004.
12. Mahafza, B. R. and M. Sajjadi, "Three-dimensional SAR imaging using linear array in transverse motion," *IEEE Trans. Aerospace and Electronic Systems*, Vol. 32, No. 1, 499–510, Jan. 1996.
13. Jun, S., X. Zhang, J. Yang, and C. Wen, "APC trajectory design for "one-active" linear-array three-dimensional imaging SAR," *IEEE Trans. on Geoscience and Remote Sensing*, Vol. 48, No. 3, 1470–1486, Mar. 2010.
14. Du, L., Y.-P. Wang, W. Hong, et al., "A three-dimensional range migration algorithm for downward-looking 3D-SAR with single-transmitting and multiple receiving linear array antennas," *EURASIP Journal on Advances in Signal Processing*, Vol. 2010, 1–15, 2010.
15. Zhang, D.-H. and X.-L. Zhang, "Downward-looking 3-D linear array SAR imaging based on chirp scaling algorithm," *2nd Asian-Pacific Conference on Synthetic Aperture Radar, APSAR 2009*, 1043–1046, 2009.

16. Shi, J., X. Zhang, J. Yang, and Y. Wang, "Surface-tracing-based LASAR 3-D imaging method via multiresolution approximation," *IEEE Trans. Geoscience and Remote Sensing*, Vol. 46, No. 11, Part 2, 3719–3730, Nov. 2008.
17. Jun, S., X. Zhang, J. Yang, and K. Liao, "Experiment results on "one-active" LASAR," *IEEE Radar Conference 2009*, 1–4, Pasadena, CA, United States, May 2009.
18. Sheen, D., D. McMakin, and T. Hall, "Near-field three-dimensional radar imaging techniques and applications," *Applied Optics*, Vol. 49, No. 19, E83–E93, Jul. 2010.
19. Balanis, C. A., *Antenna Theory: Analysis and Design*, Wiley, 1997.
20. Ward Cheney, Will light, *A Course in Approximation Theory*, Brooks/Cole, Pacific Grove, CA, 2000.
21. Koo, V. C., Y. K. Chan, V. Gobi, M. Y. Chua, C. H. Lim, C.-S. Lim, C. C. Thum, T. S. Lim, Z. Bin Ahmad, K. A. Mahmood, M. H. Bin Shahid, C. Y. Ang, W. Q. Tan, P. N. Tan, K. S. Yee, W. G. Cheaw, H. S. Boey, A. L. Choo, and B. C. Sew, "A new unmanned aerial vehicle synthetic aperture radar for environmental monitoring," *Progress In Electromagnetics Research*, Vol. 122, 245–268, 2011.
22. Wang, Y.-P., L. Du, W. Hong, et al., "Effect of linear array elements spacing on angle imaging performance of downward-looking 3D-SAR," *IGARSS 2009*, IV570–IV573, Cape Town, South Africa, Jul. 2009.
23. Wei, S.-J., X.-L. Zhang, and J. Shi, "Linear array SAR imaging via compressed sensing," *Progress In Electromagnetics Research*, Vol. 117, 299–319, 2011.
24. Freeman, A. and S. L. Durden, "A three-component scattering model for polarimetric SAR data," *IEEE Trans. on Geoscience and Remote Sensing*, Vol. 36, No. 3, 953–973, May 1998.
25. Yamaguchi, Y., T. Moriyama, M. Ishido, and H. Yamada, "Four-component scattering model for polarimetric SAR image decomposition," *IEEE Trans. on Geoscience and Remote Sensing*, Vol. 43, No. 8, 1699–1706, Aug. 2005.
26. Franceschetti, G., A. Iodice, and D. Riccio, "A canonical problem in electromagnetic backscattering from buildings," *IEEE Trans. on Geoscience and Remote Sensing*, Vol. 40, No. 8, 1787–1801, Aug. 2002.

27. Ausherman, D., A. Kozma, J. Walker, H. Jones, and E. Poggio, "Developments in radar imaging," *IEEE Trans. Aerospace and Electronic Systems*, 363, Jul. 20, 1984.
28. Socas-Navarro, H., "Polarimetric calibration of large-aperture telescopes II: The sub-aperture method," *J. Opt. Soc. Am. A*, Vol. 22, 907–912, 2005.